

Search for exotic short-range interactions using paramagnetic insulators

P.-H. Chu,^{1, 2,*} E. Weisman,³ C.-Y. Liu,³ and J. C. Long^{3, †}

¹Triangle Universities Nuclear Laboratory and Department of Physics,
Duke University, Durham, North Carolina 27708, USA

²Los Alamos National Laboratory, Los Alamos, New Mexico 87545, USA

³Department of Physics, Indiana University, Bloomington IN 47405
and IU Center for Exploration of Energy and Matter, Bloomington IN 47408

(Dated: December 3, 2024)

We describe a proposed experimental search for exotic spin-coupled interactions using a solid-state paramagnetic insulator. The experiment is sensitive to the net magnetization induced by the exotic interaction between the unpaired insulator electrons with a dense, non-magnetic mass in close proximity. An existing experiment has been used to set limits on the electric dipole moment of the electron by probing the magnetization induced in a cryogenic gadolinium gallium garnet sample on application of a strong electric field. With suitable additions, including a movable source mass, this experiment can be used to explore “monopole-dipole” forces on polarized electrons with unique or unprecedented sensitivity. The solid-state, non-magnetic construction, combined with the low-noise conditions and extremely sensitive magnetometry available at cryogenic temperatures leads to a sensitivity over ten orders of magnitude greater than existing limits in the range below 1 mm.

PACS numbers: 32.10.Dk, 11.30.Er, 77.22.-d, 14.80.Va

Introduction.— Experimental searches for macroscopic forces beyond gravity and electromagnetism have received a great deal of attention in the past two decades. Present limits allow for unobserved forces several million times stronger than gravity acting over distances of a few microns. Predictions of unobserved forces in this range have arisen in several contexts, including attempts to describe gravity and the other fundamental interactions in the same theoretical framework. For comprehensive reviews, see [1–3]. The sub-millimeter range has been the subject of active theoretical investigation, notably on account of the prediction of “large” extra dimensions at this scale which could explain the hierarchy problem [4]. The fact that the dark energy density, of order (1 meV)⁴, corresponds to a length scale of about 100 μm also encourages searches for unobserved phenomena at this scale. Many theories beyond the Standard Model possess extended symmetries that, when broken at high energy scales, give rise to light bosons with very weak couplings to matter. Examples include moduli [5], dilatons [6], and the axion—a light pseudoscalar motivated by the strong CP problem of QCD [7]. These particles can generate weak, relatively long-range interactions between samples of ordinary matter, including interactions that couple to spin. In a seminal paper [8], Moody and Wilczek derived three possible interactions for the axion, and proposed searches sensitive to the T -violating “monopole-dipole” interaction between polarized and unpolarized test masses.

We propose an experimental search for exotic spin-coupled interactions using a solid-state paramagnetic insulator as a detector. The candidate material is gadolinium

gallium garnet ($\text{Gd}_3\text{Ga}_5\text{O}_{12}$, or GGG), which has been used as a detector in an experimental search for the electric dipole moment (EDM) of the electron [9]. (See [10, 11] for realizations of other EDM materials.) In that experiment, the signal is an induced sample magnetization on application of a strong external electric field; in our proposal the magnetization is induced by an exotic monopole-dipole interaction with a dense, non-magnetic mass brought into close proximity. An exotic field coupling to the electron spins of an atom or an ion with spin $S = \sqrt{s(s+1)}$ in the solid sample leads to a net spin excess in the sample. At the location of a particular ion in the sample, the spin excess ratio is given by [12, 13]

$$R = \frac{\sum_{m_s=-s}^s m_s e^{\frac{m_s u / \sqrt{s(s+1)}}{kT}}}{\sum_{m_s=-s}^s e^{\frac{m_s u / \sqrt{s(s+1)}}{kT}}}, \quad (1)$$

where m_s is the magnetic quantum number, u is the local exotic field energy per ion, T is the sample temperature and k is Boltzmann’s constant. The resulting sample magnetization can be probed with great sensitivity using sensors based on superconducting quantum interference device (SQUID) technology.

The idea of using solid-state materials with bound but unpaired electron spins to probe exotic fields was first proposed by Shapiro in 1968 [14] in the context of EDM searches. Recently, other fundamental applications of these materials have been proposed, including tests of Lorentz and *CPT* invariance [15]. Experiments using EDM techniques, but on a different class of solid-state materials, have been proposed to search for cosmic axions [16]. Many experiments have been performed to search for spin-dependent macroscopic interactions using other methods. Examples include NMR-type exper-

* pchu@lanl.gov

† jcl@indiana.edu

iments sensitive to precession frequency shifts in various materials, including the paramagnetic salt TbF_3 [17], Hg and Cs comagnetometers [18], polarized ^{129}Xe and ^{131}Xe gas [19], and polarized 3He gas [20–22], in the presence of polarized and unpolarized masses. Other experiments search for effects in torsion pendulums [23–26], neutron bound states in the Earth’s gravitational field [27, 28], and longitudinal and transverse spin relaxation of polarized neutrons and 3He [29–33]. An overview can be found in [2]. Our proposed technique is more than 10 orders of magnitude more sensitive than current laboratory limits in the range below 1 cm, and it is sensitive to exotic interactions of electrons presently unconstrained by either laboratory experiments or astrophysical observations.

A study by Dobrescu and Mocioiu [34] of the possible interactions between non-relativistic fermions assuming only rotational invariance revealed 15 forms for the potential involving the fermion spins. Nine of these are spin-spin interactions, which would necessitate spin-polarized test masses with low intrinsic magnetism [35, 36]; here we concentrate on monopole-dipole interactions between polarized and unpolarized objects. In the zero-momentum transfer limit, the possible interactions between a polarized electron and an unpolarized atom or molecule of atomic number Z and mass A are (in SI units, and adopting the numbering scheme in [34]):

$$\begin{aligned} V_{4+5} &= (g_A^e)^2 \frac{\hbar^2}{16\pi m_e c} Z [\hat{\sigma} \cdot (\vec{v} \times \hat{r})] \left(\frac{1}{\lambda r} + \frac{1}{r^2} \right) e^{-r/\lambda}, \\ V_{9+10} &= g_P^e g_S^N \frac{\hbar^2}{8\pi m_e} A (\hat{\sigma} \cdot \hat{r}) \left(\frac{1}{\lambda r} + \frac{1}{r^2} \right) e^{-r/\lambda}, \\ V_{12+13} &= g_A^e g_V^N \frac{\hbar}{4\pi} A (\hat{\sigma} \cdot \vec{v}) \left(\frac{1}{r} \right) e^{-r/\lambda}. \end{aligned} \quad (2)$$

Here $\vec{S} = \hbar \hat{\sigma}/2$ is the electron spin, \hbar is Planck’s constant, $\hat{r} = \vec{r}/r$ is a unit vector along the direction between the electron and atom, \vec{v} is their relative velocity, c is the speed of light in vacuum, m_e is the electron mass, and λ is the interaction range. The factors g_A^e and g_V^N are the electron pseudoscalar and axial vector coupling constants, and g_S^N and g_V^N are the nucleon scalar and vector couplings. The couplings in Eq. 2 are not the most general [34]; we have included those for which the proposed experiment will have the greatest discovery potential. We note that V_{9+10} can also proceed via a spin-1 interaction, in which case the coupling is $g_A^e g_V^N$. V_{4+5} can also proceed via a spin-0 interaction, in which case the coupling is $g_S^N g_V^N$ (and the expression for V_{4+5} above is scaled by A/Z).

The experiment is illustrated schematically in Fig. 1. It is based directly on the apparatus used in [9]; many parameters have been retained for the purposes of designing a practical device. A solid paramagnetic insulating sample or “detector” mass, in the form of a block or disk, is mounted in the sample space of a large dilution refrigerator. A dense, unpolarized, non-magnetic insulator of similar size and shape is brought into close proximity and serves as “source” mass. The source-detector

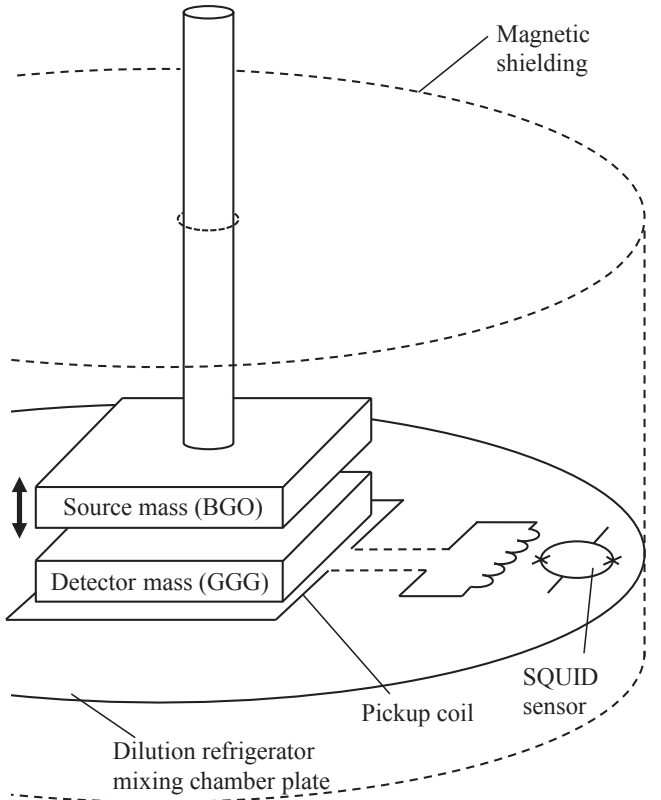


FIG. 1. Schematic of proposed experiment. A dense, non-magnetic planar source mass is modulated vertically above a paramagnetic detector mass, inducing a magnetization read out with the pickup coil and SQUID sensor. The detector is kept at sub-Kelvin temperatures.

gap can be modulated (e.g., via translation or rotation stages) from 0–1 cm with the resolution of a few microns. The non-magnetic design eliminates the need for shielding between the test masses. At closest approach, the source is essentially in contact with the detector, permitting force searches with unprecedented sensitivity in the range below 1 mm. The detector magnetization induced by the exotic interaction with the source is sensed by a pickup coil surrounding the detector. The coil is coupled to a sensitive SQUID magnetometer.

For the detector material we assume GGG, as in [9]. The use of GGG was first proposed in [37] and realized in [38]. The material is chosen to maximize the induced spin density. GGG contains a high density of Gd^{3+} ions ($\approx 10^{22}/cm^3$), each of which has seven electrons in the 4f shell: the shell is thus half-filled and all electrons are unpaired [39]. This property leads to a relatively strong magnetic response to external exotic fields. For the source mass we assume bismuth germanate ($Bi_4Ge_3O_{12}$, or BGO), a high density, non-magnetic insulator [22].

Experimental Sensitivity.— An approximate sensitivity and figure-of-merit can be derived using a simplified geometry; we examine the case of the V_{9+10} interaction,

which is the most widely studied. The interaction energy between an unpolarized, flat-plate source mass parallel to a flat-plate paramagnetic detector mass is given by:

$$U_{9+10} = g_P^e g_S^N \frac{\hbar^2}{4m_e} A_m n_m n_d S_d a_d \times \lambda^2 e^{-z(t)/\lambda} (1 - e^{-t_m/\lambda}) (1 - e^{-t_d/\lambda}), \quad (3)$$

where n_m is the number density of molecules in the source mass and A_m is their mass number, n_d is the number density of polarized ions in the detector mass and S_d is the ion spin, a_d is the detector area, $z(t)$ is the source-detector gap, and t_m and t_d are the source and detector thicknesses. This expression is exact for the case of a source of infinite area, in which case the detector spins align toward the source, in the direction normal to the detector plane. For the practical case of a finite source (considered in detail below), there are edge corrections (which are the dominant effect in the V_{4+5} case; see Eq. 2). The proposed experiment is sensitive to changes in the induced field as the source mass is modulated, which we assume to occur at some fixed frequency ω significantly above the 1/f noise corner of the SQUID. The noise corner was about 0.1 Hz for the SQUID in [9]; we assume $\omega/2\pi = 1$ Hz. From Fourier analysis, the amplitude of the energy change per detector ion at ω is

$$\tilde{u}_{9+10} = A_m g_P^e g_S^N \frac{\hbar^2}{2m_e} n_m S_d \lambda I_1(z_0/\lambda) e^{-\bar{z}/\lambda} (1 - e^{-t_m/\lambda}), \quad (4)$$

where $\tilde{u}_{9+10} = \tilde{U}_{9+10}/N_d$ and $N_d = n_d a_d t_d$ is the number of detector spins. In Eq. 4 we have taken the limit $\lambda \gg t_d$, so that \tilde{u}_{9+10} is a good approximation at the location of any particular ion in the detector mass (or, equivalently, in a layer of thickness $\approx \lambda$ at the top surface of a thicker detector). Here, $I_1(z_0/\lambda)$ is the modified Bessel function, and we have used $z(t) = \bar{z} + z_0 \sin \omega t$ where $\bar{z} = (z_{\max} + z_{\min})/2$ is the average source-detector gap and $z_0 = (z_{\max} - z_{\min})/2$ is the amplitude of the source mass motion.

In the limit $\tilde{u}_{9+10} \ll kT$, the spin excess ratio (Eq. 1) can be approximated as $R = \tilde{u}_{9+10}/(3kT)$, whereby the total spin excess in the layer is $S_d N_d \tilde{u}_{9+10}/(3kT)$. The layer magnetization normal to the plane is

$$M = \frac{g\mu_B S_d n_d \tilde{u}_{9+10}}{3kT}, \quad (5)$$

where $g = 2$ for electrons and μ_B is the Bohr magneton. The induced magnetic flux in a pickup coil of area a_c near the detector is then $\Phi_i = \mu_0 f M a_c$, where μ_0 is the permeability of free space. This will be nearly optimal for a coil with $a_c \approx a_d$ surrounding the midplane of the detector, but we include a suppression factor f for sub-optimal coupling between the detector and coil.

In an experiment using a practical SQUID sensor, the pickup coil connects to a built-in input coil on the sensor. The changing flux from the detector induces a current, which flows into the input coil and produces a flux that

couples inductively to the SQUID loop and is transduced to a voltage. The relationship between the magnetic flux Φ_i picked up from the detector mass and the induced flux Φ_{sq} in the SQUID loop is [9]

$$\Phi_{sq} = \frac{M}{L_p + L_i} \Phi_i = \beta \Phi_i, \quad (6)$$

where L_p and L_i are the inductances of the pickup and input coils, respectively, and M is the mutual inductance between the input coil and SQUID. The factor β is the coupling efficiency which quantifies the flux reduction when Φ_i is delivered to the SQUID sensor.

The sensitivity of the experiment is based on the expectation that essentially all backgrounds can be suppressed below the intrinsic noise of the SQUID sensor. In an experiment limited by this noise (ϕ_n , expressed in terms of magnetic flux per root bandwidth), the signal-to-noise ratio is given by:

$$SNR = \frac{\Phi_{sq} \sqrt{\tau}}{\phi_n}, \quad (7)$$

where τ is the integration time. The sensitivity is calculated by setting $SNR = 1$ and solving for $g_P g_S$. Combining Eqs. 3 through 7, the result is:

$$g_P^e g_S^N = \frac{4\mu_B m_e u}{\hbar^2} \frac{1}{\rho_m} \frac{1}{\lambda \epsilon} \frac{1}{\beta f} \frac{\phi_n}{\sqrt{\tau}} \frac{1}{a_d} \left(\frac{1}{\chi_d} + D \right). \quad (8)$$

Here we have used $n_m = \rho_m/(u A_m)$, where ρ_m is the mass density of the source and u is the atomic mass unit. The factor χ_d is the effective susceptibility of the detector mass:

$$\chi_d = \frac{4\mu_0 \mu_B^2 n_d S_d^2}{3kT}, \quad (9)$$

and we have used $\chi_d \rightarrow \chi_d/(1 + D\chi_d)$ in Eq. 8, where D is the demagnetization factor. The efficiency $\epsilon \equiv I_1(z_0/\lambda) e^{-\bar{z}/\lambda} (1 - e^{-t_m/\lambda})$ in Eq. 8 is of order unity for an optimized vertical geometry.

A plot of $g_P^e g_S^N$ vs λ from Eq. 8 is shown in Fig. 3, using the parameters in Tables I and II. We assume the source and detector can be brought into contact but also that these elements can only be made flat to within a few microns, thus the minimum gap is set to 10 μm . For each value of λ , the maximum separation z_{\max} is chosen to maximize ϵ , which occurs around $z_{\max} = 3\lambda$. The efficiency is maximized for $t_m \rightarrow \infty$, however, since very little is gained for $t_m > \lambda$, we set $t_m = 1$ cm, about twice the maximum range of interest. A suppression factor of $f = 0.4$ has been used, in accordance with [9]. For a rectangular prism of square cross-section a_d magnetized parallel to the thickness (here $\approx \lambda$), we have used the approximation $D \approx \sqrt{a_d}/(\sqrt{a_d} + 2\lambda)$ [40].

From Eq. 8, an approximate figure-of-merit for the experiment is:

$$FOM = \rho_m \epsilon a_d \beta f \frac{\sqrt{\tau}}{\phi_n} \frac{\chi_d}{1 + D\chi_d}, \quad (10)$$

illustrating the importance of high ρ_m , and $\bar{z} \approx z_0 \approx \lambda$ (through ϵ). Over the range of interest, D varies between 0.75 and 1. Thus it is important that χ_d be at least of order unity, but larger values will yield little improvement for the chosen detector geometry. We note Eq. 9 suggests χ_d could be improved by several orders of magnitude by operation at the sub-Kelvin temperatures available in dilution refrigerators. However, as discussed in [9], the susceptibility of practical paramagnetic insulators is well described by a Curie-Weiss relation of the form $\chi = C/(T - T_{CW})$, where $|T_{CW}|$ represents an effective minimum temperature assuming the operating temperature is lower. Following [9], we use $T_{CW} = -2.1$ K. We assume an operating temperature of 1.0 K, the lowest temperature at which the susceptibility obeys the Curie-Weiss law [41]. This leads to an effective temperature of $T = 3.1$ K in Eq. 9 and an estimate of $\chi_d = 0.53$ (Table I), slightly below the value measured in [41] for single-crystal GGG. Optimization of other terms in Eq. 10 is discussed below.

TABLE I. Parameters used in the sensitivity computation.

Parameter	Value
effective area of pickup coil, a_c	12.75 cm ²
source mass density (BGO), ρ_m	7.13 g/cm ³
detector spin density, n_d	10 ²² /cm ³
detector spin/Gd ion, s	7/2
detector susceptibility, χ_d	0.53 (SI)
coupling efficiency, β	7.8 × 10 ⁻³
sensor intrinsic noise, ϕ_n	3 $\mu\Phi_0/\sqrt{\text{Hz}}$
integration time, τ	10 ⁶ s

TABLE II. Dimensions of the detector and source masses used in the sensitivity calculations.

Parameter	Value
detector width, x_d	3.00 cm
detector length, y_d	3.00 cm
detector thickness, z_d	0.76 cm
source mass width, x_m	3.00 cm
source mass length, y_m	3.00 cm
source mass thickness, z_m	1.00 cm
minimum gap, z_{min}	10 μm

For more accurate estimates of the sensitivity of a practical experiment to each potential in Eq. 2, we perform numerical calculations, in which all approximations used above are relaxed. The theoretical interactions from each potential due to a finite-sized source are computed at representative points in a hypothetical, practically-shaped detector and used to generate a spin excess profile as a function of the spatial coordinates. This profile is then used in a finite element (FEA) model to create a map

of the induced flux Φ_i in the region of the detector and pickup coil.

The detector is broken up into subvolumes and the potentials calculated by Monte Carlo integration between the center point of each subvolume and the complete volume of the source mass. The detector and source dimensions (very similar to those used for the sample in [9]) are given in Table II. The induced spin orientation at each subvolume location is obtained by repeating the calculation for many possible orientations and taking the maximum. The integration models the modulation of the source mass (assumed sinusoidal) and records the results at several values of the separation (that is, the source phase) over a complete period. A minimum source-sample gap of 10 μm is used as in the analytical estimate. The maxima are then converted to magnetization vectors for each subvolume and phase using Eq. 1 and the parameters in Table I. Fig. 2 shows a detector magnetization map for the case of the V_{9+10} interaction with $\lambda = 5$ mm at a particular source phase.

Magnetization maps are then entered into an electromagnetic FEA model of the sample generated with the COMSOL software package [42]. The model interpolates between the points of the input data to generate a complete magnetization profile within the detector volume and a complete field profile in the interior and exterior. An example field profile is shown in Fig. 2.

From these profiles, the flux through the area of the pickup coils in the proposed experiment is calculated. Following [9], we assume a planar gradiometer design for the pickup coil for the V_{9+10} and V_{12+13} interactions, to reduce common-mode backgrounds; the coil area in Table I matches that in [9]. For the V_{4+5} interaction, the coil takes the planar “figure-8” form shown in Fig. 2 for similar common-mode rejection, either sandwiched between two halves of a split detector or wound through a small vertical hole in the center. For a particular interaction in Eq. 2 at a given range λ , the experimental signal is calculated by taking the Fourier transform of the flux through the gradiometer coil as a function of the source phase, and scaling the result by the reduction factor in Eq. 6. For each value of λ investigated, the source mass amplitude is optimized for maximum signal, resulting in amplitudes of order λ . Finally, the SNR is obtained by dividing this result by the sensor intrinsic noise (Table I). The coupling constants in Eq. 2 are then adjusted so that $SNR = 1$, resulting in the sensitivity curves in Fig. 3.

The velocity-dependent interactions V_{4+5} and V_{12+13} are *unconstrained* for the case of polarized electrons. (We note that, if V_{4+5} is interpreted exclusively as an axial-vector interaction, the coupling $(g_A^e)^2$ is tightly constrained by electron spin-spin experiments [35, 43, 44].) For rough comparison, the bold solid line in the V_{4+5} plot is the limit on the corresponding coupling for polarized nucleons from the experiment at the Paul Scherrer Institute [45]; the long-dashed line is the preliminary limit on the nucleon coupling from [46]. Similarly, the bold solid line in the V_{12+13} plot is the limit on the corresponding

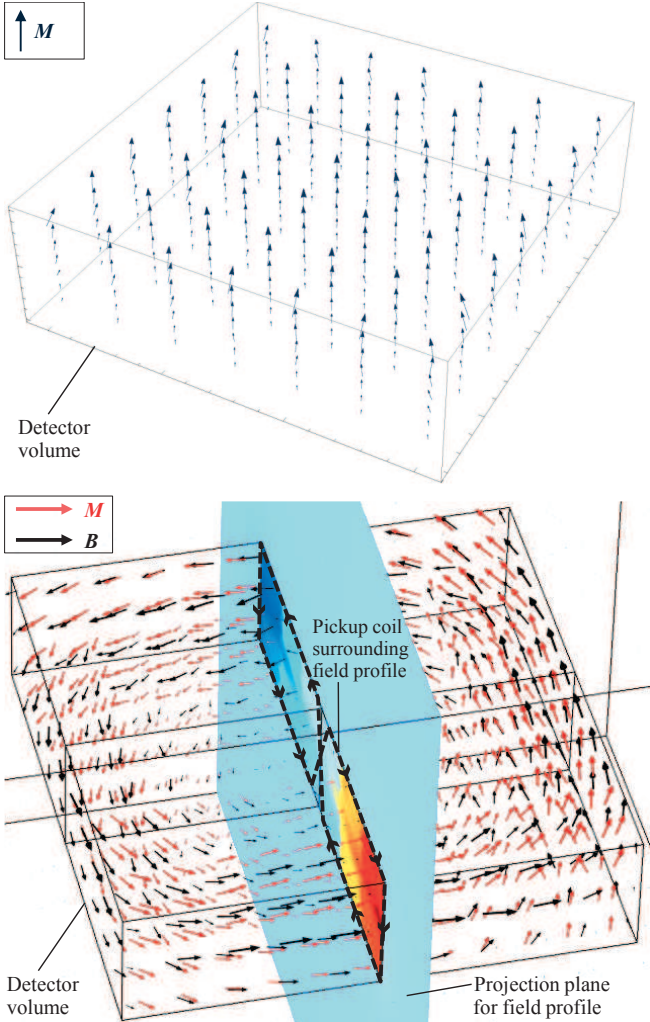


FIG. 2. (Color online) *Top*: map of detector mass magnetization induced by source in V_{9+10} interaction. Vectors represent magnetization (each an average of one of 343 subvolumes). *Bottom*: magnetization (light arrows) and magnetic field (black arrows) induced by source in V_{4+5} interaction. Flux is calculated through cross section; dotted line shows placement of pickup coil for V_{4+5} experiment. In both cases $\lambda = 5$ mm, and source (not shown) is slab of identical area centered above detector at instantaneous separation of 3 mm.

polarized nucleon coupling derived from the neutron spin rotation experiment at NIST [47].

The best limit on the V_{9+10} interaction for electrons derives from the axionlike particle torsion pendulum in the Eot-Wash group [26]. This limit is indicated by the bold line in the V_{9+10} plot; the dotted line below it is the projected thermal limit. The sensitivity of the proposed experiment ranges from two to over ten orders of magnitude greater in the range of interest. It is slightly lower than the analytical estimate from Eq. 8, likely on account of the approximation of an infinite-area source in that estimate.

The fine solid lines in the V_{4+5} and V_{9+10} plots are

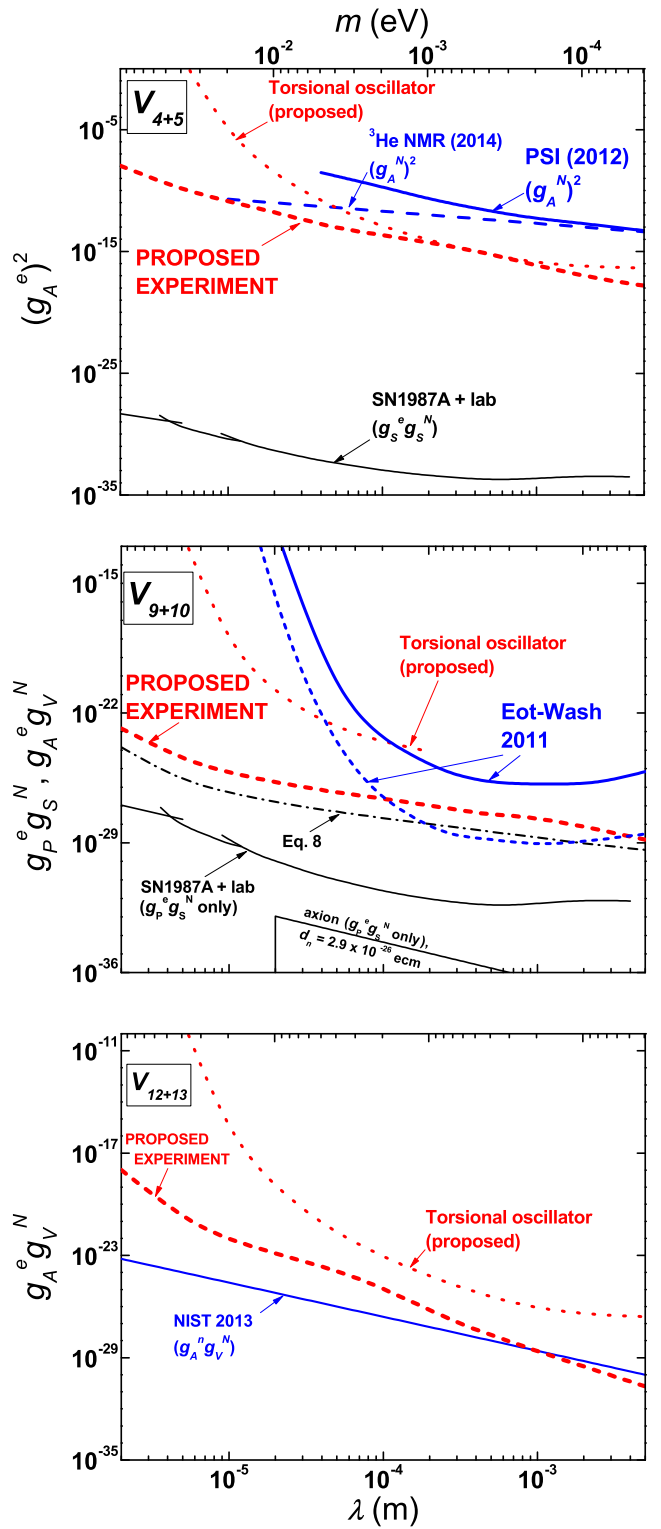


FIG. 3. (Color online) Projected sensitivity of proposed experiment to V_{4+5} , V_{9+10} , and V_{12+13} interactions, in which couplings are plotted versus range λ (lower axes) or mass of unobserved boson (upper axes). Bold solid (dashed) curves are current (preliminary) limits, fine solid curves are indirect limits, dotted curves are proposals, dot-dash curve is Eq. 8. See text for explanations.

the limits obtained from combining the constraints on g_S^e or g_P^e from the inferred cooling rate of SN1987A with the constraints on g_S^N from spin-*independent* short-range fifth force experiments [48]. These apply to spin-0 interactions and are thus for illustrative purposes only in case of V_{4+5} . The V_{9+10} limits are still more stringent than the projections for the direct search proposed, though the latter are more general and free from uncertainties related to dense nuclear matter effects in stars.

The V_{9+10} plot also shows the limit inferred from the constraint on the electric dipole of the neutron (d_n) [49], which sets bounds on g_S^N via the QCD θ -term, thus is restricted to case of the (spin-0) axion. For generic light scalars unrelated to the strong CP problem, the limits from direct searches are more stringent than those inferred from EDM bounds over the range of interest [50]. Thus, correlating observations in EDM and macroscopic experiments could help distinguish axions from more generic light scalars.

The light dotted lines in each plot are the projected sensitivity of the proposed experiment in [36]. That proposal is sensitive to polarized electron coupling and competes directly, but our projections are stronger by about 1-10 orders of magnitude for all interactions. A proposal for a direct experiment sensitive to the axion region in the V_{9+10} plot is described in [51], though that experiment is sensitive to polarized nucleon coupling.

Backgrounds.— The analysis above assumes the sensitivity of the experiment to be limited by the intrinsic noise of the SQUID sensor. Both GGG and BGO are good electrical insulators so Johnson noise levels are expected to be very low, however, magnetic noise due to dissipation in the test masses is another possible statistical background. The spectral density of magnetization noise in the detector mass is given by [10, 52]:

$$M_\omega \approx \frac{1}{\mu_0} \sqrt{\frac{kT\mu''}{V\omega}}, \quad (11)$$

where V is the volume and μ'' is the imaginary part of the complex permeability. While data on μ'' for the proposed GGG detector material are not available, it is expected to be too small (and even smaller in BGO, which has much lower susceptibility) for this noise to be observable. It was not observed, for example, in the experiment in [9], results from which were consistent with SQUID noise after 5 days of integration time.

Systematic effects are a greater concern. For example, the source can acquire a magnetization $M_m = \chi_m B_0 / \mu_0$ via the interaction of its susceptibility χ_m with a stray field B_0 . The changing flux through the pickup coil as the source oscillates above it can mimic a signal. BGO is diamagnetic with $\chi_m = -1.9 \times 10^{-5}$ at room temperature [53], however there is evidence that it is weakly paramagnetic in low fields. Low-temperature data on χ_m of pure BGO are not available, but the related compound $\alpha\text{-Bi}_2\text{O}_3$ exhibits $\chi_m \approx 1.8 \times 10^{-6}$ at 4 K in low fields [54]. We estimate the flux as $d\phi \approx (\partial B / \partial z) z_0 a_d$,

where $\partial B / \partial z$ is the gradient above the center of a magnetized disk of area a_d a distance z_d above the coil (Table II), and z_0 is the largest source amplitude. Requiring $d\phi < \phi_n / \sqrt{\tau}$ leads to an upper limit on the allowed stray field of $B_0 \approx 10^{-12}$ T. Assuming typical stray laboratory fields on the order of 10^{-4} T, the required shielding factor is 10^8 . This is quite modest compared to the experiment in [9], which used two layers of superconducting lead foils and three layers of mu-metal sheets wound on frames to attain a measured shielding factor of 5×10^{11} (which we assume here).

Vibrations are potentially more troublesome. Motion of the detector-pickup coil assembly in phase with the source drive can lead to a signal in the presence of a stray gradient $\partial B_0 / \partial z$, given by $d\phi \approx (\partial B_0 / \partial z) \delta z_d a_d$, where δz_d is the assembly vibration amplitude. This signal is common-mode; the common-mode rejection ratio of the pickup coil used in [9] was about 2×10^2 . Dividing the estimate for $d\phi$ by this factor and again demanding $d\phi < \phi_n / \sqrt{\tau}$ leads to a requirement on the stray gradient of $\partial B_0 / \partial z < 10^{-12}$ T/m per micron of assembly vibration. Assuming typical lab gradients of order 10^{-3} T/m, this is within the shielding factor for vibrations less than about $100 \mu\text{m}$. If the vibrations cause the assembly to tilt in a stray field of 10^{-12} T, the resulting flux signal will be below the noise if the vibrations are less than about $30 \mu\text{m}$. These effects can be studied by examining signals in the absence of a detector mass. The simple translating source mass assumed can be replaced by a rotor with several segments of alternating density that pass over the detector at a multiple of the rotary drive frequency [51, 55], thus decoupling the drive frequency from the actual source modulation.

Conclusions.— We have performed detailed calculations of the projected sensitivity of an exotic interaction search with a paramagnetic insulating detector at cryogenic temperatures. The proposed technique affords the possibility to probe the interaction between macroscopic test masses in near contact in a low-noise environment. Our results indicate either unique sensitivity to electron “monopole–dipole” interactions in the range below 1 mm, or ultimate improvements of more than ten orders of magnitude over existing experiments. The proposed technique is based largely on a proven design. Our primary purpose has been to show the potential sensitivity of that design, especially with the parameters of the existing detection scheme. Technical challenges associated with source mass translation in the cryostat and the related systematic backgrounds will certainly have to be addressed. Possible improvements include better SQUID coupling efficiency (β in Eq. 10), though this is a subtle optimization problem [10]. Increasing the detector area a_d (on which the dependence of Eq. 10 is essentially linear, given the near saturation of the demagnetization factor) is another possibility, though problems of test mass metrology and changes to SQUID coupling efficiency will warrant careful study.

Acknowledgments.— The authors thank H. Gao, E.

Smith, A. Holley, and W. M. Snow for useful discussions. This work is supported by National Science Foundation

Grants PHY-1207656, PHY-1306942, Duke University, Los Alamos National Laboratory, and the Indiana University Center for Spacetime Symmetries (IUCSS).

[1] E. Adelberger, J. Gundlach, B. Heckel, S. Hoedl, and S. Schlamminger, *Prog. Part. Nucl. Phys.* **62**, 102 (2009).

[2] I. Antoniadis, S. Baessler, M. Buchner, V. Fedorov, S. Hoedl, *et al.*, *Comptes Rendus Physique* **12**, 755 (2011).

[3] J. Jaeckel and A. Ringwald, *Ann. Rev. Nucl. Part. Sci.* **60**, 405 (2010), arXiv:1002.0329 [hep-ph].

[4] N. Arkani-Hamed, S. Dimopoulos, and G. Dvali, *Phys. Lett.* **B429**, 263 (1998), arXiv:hep-ph/9803315 [hep-ph].

[5] S. Dimopoulos and A. A. Geraci, *Phys. Rev.* **D68**, 124021 (2003), arXiv:hep-ph/0306168 [hep-ph].

[6] D. B. Kaplan and M. B. Wise, *JHEP* **0008**, 037 (2000), arXiv:hep-ph/0008116 [hep-ph].

[7] R. D. Peccei and H. R. Quinn, *Phys. Rev. Lett.* **38**, 1440 (1977).

[8] J. E. Moody and F. Wilczek, *Phys. Rev.* **D30**, 130 (1984).

[9] Y. Kim, C.-Y. Liu, S. Lamoreaux, G. Visser, B. Kunkler, *et al.*, arXiv:1104.4391 [nucl-ex].

[10] A. O. Sushkov, S. Eckel, and S. K. Lamoreaux, *Phys. Rev. A* **79**, 022118 (2009).

[11] S. Eckel, A. O. Sushkov, and S. K. Lamoreaux, *Phys. Rev. Lett.* **109**, 193003 (2012), arXiv:1208.4420 [physics.atom-ph].

[12] C. Kittel and H. Kroemer, *Thermal Physics*, 2nd ed. (W. H. Freeman, 1980) p. 70.

[13] A. Abragam, *The Principles of Nuclear Magnetism* (Oxford, 1978) p. 2.

[14] F. L. Shapiro, *Sov. Phys. Usp.* **11**, 345 (1968).

[15] R. Bluhm and V. A. Kostelecky, *Phys. Rev. Lett.* **84**, 1381 (2000), arXiv:hep-ph/9912542 [hep-ph].

[16] D. Budker, P. W. Graham, M. Ledbetter, S. Rajendran, and A. O. Sushkov, *Phys. Rev. X* **4**, 021030 (2014), arXiv:1306.6089 [hep-ph].

[17] W.-T. Ni, S.-S. Pan, H.-C. Yeh, L.-S. Hou, and J.-L. Wan, *Phys. Rev. Lett.* **82**, 2439 (1999).

[18] A. N. Youdin, D. Krause, K. Jagannathan, L. R. Hunter, and S. K. Lamoreaux, *Phys. Rev. Lett.* **77**, 2170 (1996).

[19] M. Bulatowicz, R. Griffith, M. Larsen, J. Mirijanian, T. Walker, *et al.*, *Phys. Rev. Lett.* **111**, 102001 (2013), arXiv:1301.5224 [physics.atom-ph].

[20] G. Vasilakis, J. M. Brown, T. W. Kornack, and M. V. Romalis, *Phys. Rev. Lett.* **103**, 261801 (2009), arXiv:0809.4700 [physics.atom-ph].

[21] P. Chu, A. Dennis, C. Fu, H. Gao, R. Khatiwada, *et al.*, *Phys. Rev.* **D87**, 011105 (2013), arXiv:1211.2644 [nucl-ex].

[22] K. Tullney, F. Allmendinger, M. Burghoff, W. Heil, S. Karpuk, *et al.*, *Phys. Rev. Lett.* **111**, 100801 (2013), arXiv:1303.6612 [hep-ex].

[23] R. C. Ritter, L. I. Winkler, and G. T. Gillies, *Phys. Rev. Lett.* **70**, 701 (1993).

[24] G. D. Hammond, C. C. Speake, C. Trenkel, and A. P. Paton, *Phys. Rev. Lett.* **98**, 081101 (2007).

[25] B. R. Heckel, E. Adelberger, C. Cramer, T. Cook, S. Schlamminger, *et al.*, *Phys. Rev.* **D78**, 092006 (2008), arXiv:0808.2673 [hep-ex].

[26] S. A. Hoedl, F. Fleischer, E. G. Adelberger, and B. R. Heckel, *Phys. Rev. Lett.* **106**, 041801 (2011).

[27] S. Baessler, V. V. Nesvizhevsky, K. V. Protasov, and A. Y. Voronin, *Phys. Rev.* **D75**, 075006 (2007), arXiv:hep-ph/0610339 [hep-ph].

[28] T. Jenke, G. Cronenberg, J. Burgdorfer, L. Chizhova, P. Geltenbort, *et al.*, *Phys. Rev. Lett.* **112**, 151105 (2014), arXiv:1404.4099 [gr-qc].

[29] A. Serebrov, *Phys. Lett.* **B680**, 423 (2009), arXiv:0902.1056 [nucl-ex].

[30] Y. Pokotilovski, *Phys. Lett.* **B686**, 114 (2010), arXiv:0902.1682 [nucl-ex].

[31] A. K. Petukhov, G. Pignol, D. Jullien, and K. H. Andersen, *Phys. Rev. Lett.* **105**, 170401 (2010), arXiv:1009.3434 [physics.atom-ph].

[32] C. B. Fu, T. R. Gentile, and W. M. Snow, *Phys. Rev.* **D83**, 031504 (2011).

[33] A. K. Petukhov, G. Pignol, and R. Golub, *Phys. Rev.* **D84**, 058501 (2011), arXiv:1103.1770 [hep-ph].

[34] B. A. Dobrescu and I. Mocioiu, *JHEP* **0611**, 005 (2006), arXiv:hep-ph/0605342 [hep-ph].

[35] R. C. Ritter, C. E. Goldblum, W.-T. Ni, G. T. Gillies, and C. C. Speake, *Phys. Rev. D* **42**, 977 (1990).

[36] T. M. Leslie, E. Weisman, R. Khatiwada, and J. C. Long, *Phys. Rev.* **D89**, 114022 (2014), arXiv:1401.6730 [hep-ph].

[37] S. K. Lamoreaux, *Phys. Rev.* **A66**, 022109 (2002), arXiv:nucl-ex/0109014 [nucl-ex].

[38] C.-Y. Liu and S. Lamoreaux, *Mod. Phys. Lett.* **A19**, 1235 (2004).

[39] S. Geller, in *Physics of magnetic garnets*, Vol. Proc. Intl. School Phys. “Enrico Fermi,” Course LXX, edited by S. Geller and A. Paoletti (Societ`a Italiana di Fisica, Bologna, 1978) p. 1.

[40] M. Sato and Y. Ishii, *Journal of Applied Physics* **66**, 983 (1989).

[41] P. Schiffer, A. P. Ramirez, D. A. Huse, P. L. Gammel, U. Yaron, D. J. Bishop, and A. J. Valentino, *Phys. Rev. Lett.* **74**, 2379 (1995).

[42] *Comsol, Version 4.4*, Comsol, Inc., 1 New England Executive Park, Burlington, MA 01803 USA.

[43] B. R. Heckel, W. A. Terrano, and E. G. Adelberger, *Phys. Rev. Lett.* **111**, 151802 (2013).

[44] S. Kotler, R. Ozeri, and D. F. J. Kimball, arXiv:1501.07891 [physics.atom-ph].

[45] F. M. Piegsa and G. Pignol, *Phys. Rev. Lett.* **108**, 181801 (2012), arXiv:1205.0340 [hep-ex].

- [46] Y. Zhang, G. Sun, S. Peng, C. Fu, H. Guo, *et al.*, arXiv:1412.8155 [nucl-ex].
- [47] H. Yan and W. M. Snow, Phys. Rev. Lett. **110**, 082003 (2013), arXiv:1211.6523 [nucl-ex].
- [48] G. Raffelt, Phys. Rev. **D86**, 015001 (2012), arXiv:1205.1776 [hep-ph].
- [49] C. Baker, D. Doyle, P. Geltenbort, K. Green, M. van der Grinten, *et al.*, Phys. Rev. Lett. **97**, 131801 (2006), arXiv:hep-ex/0602020 [hep-ex].
- [50] S. Mantry, M. Pitschmann, and M. J. Ramsey-Musolf, Phys. Rev. **D90**, 054016 (2014), arXiv:1401.7339 [hep-ph].
- [51] A. Arvanitaki and A. A. Geraci, Phys. Rev. Lett. **113**, 161801 (2014), arXiv:1403.1290 [hep-ph].
- [52] S. Eckel, A. O. Sushkov, and S. K. Lamoreaux, Phys. Rev. B **79**, 014422 (2009).
- [53] S. Yamamoto, K. Kuroda, and M. Senda, IEEE Trans. Nucl. Sci. **50**, 1683 (2003).
- [54] E. Kravchenko, V. Orlov, and M. Shlykov, Russ. Chem. Rev. **75**, 77 (2006).
- [55] Y. J. Chen, W. Tham, D. Krause, D. Lopez, E. Fischbach, *et al.*, arXiv:1410.7267 [hep-ex].